Resonant coherent excitation and energy loss of slow channeling helium ions in AlN

Chang-Kai Li [1], Jian-ming Xue,[1,*] Xiao-ping OuYang [2,3] and Feng-Shou Zhang [3,4,5,†]

[1]*State Key Laboratory of Nuclear Physics and Technology, School of Physics, Peking University, Beijing 100871, China*

[2]*Northwest Institute of Nuclear Technology, Xian 710024, China*

[3]*The Key Laboratory of Beam Technology and Material Modification of Ministry of Education, College of Nuclear Science and Technology, Beijing Normal University Beijing 100875, China*

[4]*Beijing Radiation Center, Beijing 100875, China*

[5]*Center of Theoretical Nuclear Physics, National Laboratory of Heavy Ion Accelerator of Lanzhou, Lanzhou 730000, China*

(Received 21 September 2021; revised 19 December 2021; accepted 14 January 2022; published 28 January 2022)

By performing real-time time-dependent density-functional theory dynamic simulations, we report a velocity-dependent charge resonance on slow initial bare ions when channeling through the rocksalt crystalline AlN. Such charge resonance is accompanied by tremendously enhanced stopping at narrow velocity windows, which is attributed to the depletion in electronic screening by bound electrons, when the formation of defect state on projectile is depressed dramatically by the periodical field from lattice arrangement. The enhancement of stopping is not found in simulations with initial neutral incident ion, suggesting the effect of such charge resonance process mainly resides in the charge accumulation during the preequilibrium state, while making marginal influence on the excitation of bound state charge. We also investigated the charge resonance with revised lattice parameter, confirming the periodic atomic arrangement of lattice plane along ion trajectory is the main cause of such charge resonance.

DOI: 10.1103/PhysRevA.105.012819

I. INTRODUCTION

Along high symmetry directions in a crystal lattice, a swift moving ion can travel large distances in a process known as channeling. For example, a 40 keV Xe ion can reach μm depths in crystalline tungsten, but only 0.02 μm in the amorphous form [1]. This channeling phenomenon has attracted the attention of many researchers in the field of ion implantation, since channeled-ion implantation provides more advantages compared with conventional implantation along the random direction (random implantation) such as less radiation damage, deeper doping for the same energy, and less lateral spread of implanted ions [2]. Nevertheless, channeling is a double-edged sword, it brings trouble in the field of radiation shielding, where incident high-energy neutrons in a reactor may displace host atoms exceptionally large distances, significantly increasing the size of the damaged region [3]. Accurate knowledge of the energy deposition by energetic charged particles in matter is imperative for understanding channeling phenomena [4,5] and the associated applications [6,7].

Since energetic ions impinging on a surface and aligned with low-index crystallographic axes or planes can travel considerable distances avoiding head-on collisions with a host nucleus [8]. The kinetic energy loss involved in the ion channeling process is mainly transferred to the electronic system, the dissipative force thus generated is called the electronic stopping power S_e.

The material studied in this work is rocksalt crystalline AlN impacted by helium ions at low projectile velocities. For semiconductors and insulators, it has been suggested that there is a threshold velocity below which a light projectile would not cause electronic excitation. The electronic stopping would be strictly zero below this threshold. Above the threshold velocity, the stopping in insulator shows a metal-like behavior, and is insensitive to the band gap. Up to now, the threshold effects are mainly found for proton colliding with insulator [9,10], for heavier projectile, even the helium ion [11], threshold effect is weaken by the defect level caused by the intruding ion either served as intermediate level reducing the band gap [12] or as electron elevator transferring the electron between the valence and conduct band [13].

Common analytic models for S_e include Lindhard-Winther theory [14], which describes the electronic excitations via linear plasmonic response. In this model electronic stopping depends quadratically on the effective charge Z_{eff} of the projectile with velocity v, and increases with the electron density n of the target material,

$$-\frac{dE}{dx} = \frac{4\pi}{m}\left(\frac{Z_{\text{eff}}e^2}{v}\right)^2 nL(v,n), \tag{1}$$

$L(v,n)$ is the stopping number, describing the linear plasmonic response of the free electron gas (FEG), which can be calculated as a double integral in energy and momentum of the energy-loss function using, e.g., the random-phase approximation [15,16]. Alternatively, electronic stopping can be

*Corresponding author: jmxue@pku.edu.cn

†Corresponding author: fszhang@bnu.edu.cn

calculated using binary collision theory formulation. Early versions, such as the Bethe formulation [17], treat the scattering events (semi)classically. Along with the development of quantum mechanics, many-body effects such as electronic screening were included; one example is the Lindhard-Scharff theory [18]. At low velocities, with ionic energies below stopping maximum, a first-order approximation of this theory shows that S_e is linearly proportional to the incident particle velocity, and dependent on the charge state [19,20] of the channeling ion. Similar linear velocity dependence of S_e is also arrived at in Lindhard-Winther theory for low velocities.

However, analytical versions of both approaches [14,16,18] require the effective charge of the projectile and the number of electrons involved in the electronic excitation as external parameters [15]. In particular, Bethe-Bloch or Lindhard-Winther approaches assume that the target material is amorphous, which entirely neglects any impact of the crystalline structure and local electron density. In going beyond analytical models, an important milestone was the advent of density-functional theory (DFT), which takes into account the energy dissipation, electron density fluctuation, induced screened potential, in a self-consistent way [21,22], since then the fully *ab initio* evaluation of the electronic stopping power has become within reach. Furthermore, beyond the FEG approximation, recent development of DFT [23–25] explicitly takes into account the effects of inhomogeneity in electron density due to the underlying lattice structure, band structure and band gap.

Present theoretical and experimental research works with target structure taken into account mainly focus on the effect of impact parameter [23,26,27] and incident angle [28,29] on electronic stopping power, while there are few studies about the structural dependence of the electron stopping power in low-velocity regime.

In 1978, Datz *et al.* [30] observed resonant peaks in the probability of excitation processes for swift channeling ions with energies above 1.5 MeV/u in silver and gold crystals. Such resonances were predicted by Okorokov [31] to occur when the lattice potential sensed by the channeling ion, periodic in time and space, stimulates electronic transitions between its core states, resulting in the presence of inner-shell vacancies on the projectile ions [32,33]. The situation for slow ion is much more complicated, since characteristic excitation energy lies within the valence band of the ion, charge transfer and screening effect of bound charge are hence revelent. These resonant excitations are crystal-structure-related aspects of channeling, which cannot be predicted within the standard framework of ions traveling through free electron gas or colliding with isolated atom.

In this work, we demonstrate, through time-dependent density-functional theory (TDDFT) coupling Ehrenfest molecular dynamics (EMD) [34], that the electronic screening affects the energy loss of the slow channeling helium ions, which are partially neutralized in a nontrivial manner: S_e shows a specific dependence on the charge state of the projectile. We also report a velocity-dependent charge resonance phenomenon, which results from the periodical field from an array of the atomic planes, and significantly suppresses the charge accumulation on the highly charged channeling ion within narrow velocity windows.

This paper is outlined as follows. In Sec. II, we briefly introduce the theoretical framework and the computational details. Results are presented and discussed in Sec. III, where we concentrate on the following three parts: we first discuss in detail the effect of charge screening on S_e and a charge resonance phenomenon induced by the periodical field from atomic planes in Sec. III A; then in Sec. III B, we present the S_e and the charge states for initial neutral incident ions; in the end, we make analysis of the lattice parameter dependence of charge resonance in Sec. III C. Conclusions are drawn in Sec. IV.

II. MODEL AND METHODS

During the course of the simulation, we monitored the energy transferred to the electrons of the target due to a constant velocity moving helium ion. For simplicity, and since the S_e is a velocity-resolved quantity, the intruder is constrained to move at given velocity, hence the total energy of the system is not conserved. The excess in total energy is instead used as a measure of the stopping power as a function of the projectile velocity. As the incident ion moves, the time-dependent Kohn-Sham (TDKS) equation describes the evolution of the electronic density and energy of the system, due to the dynamics of effective single-particle states under the external potential generated by the helium ion and the crystal of host nuclei. These states are evolved in time with a self-consistent Hamiltonian that is a functional of the density:

$$i\hbar\frac{\partial\varphi_i(\vec{r},t)}{\partial t}=\left[-\frac{\hbar^2\nabla^2}{2m}-V_{KS}\right]\varphi_i(\vec{r},t), \tag{2}$$

with

$$V_{KS}=-\sum_I\frac{Z_I}{|\vec{R}_I(t)-\vec{r}|}+\int\frac{n(\vec{r'},t)}{|\vec{r}-\vec{r'}|}d\vec{r'}+V_{xc}(\vec{r'},t), \tag{3}$$

$\varphi_i(\vec{r},t)$ being occupied orbital for the ith electron. V_{xc} is the time-dependent exchange-correlation potential, which is initially a functional of the density $n(\vec{r'},t')$ at all points $\vec{r'}$ and at all times $t'<t$. Since the adiabatic approximation is exploited in this work, the memory effects of V_{xc} are not taken into account, V_{xc} is only a functional of $n(\vec{r'},t)$ at the current time t. The other two terms of V_{KS} are the electron-nucleus potential, and the Hartree potential, respectively. In the present work, we mainly focus on the ion-solid interaction under well-channeled condition with projectile velocity below 1 atomic unit (a.u.), only valence electrons of the host atoms ($3p$ for aluminum and $2s3p$ for nitrogen) are explicitly included, the coupling of valence electrons to ionic cores is described by using norm-conserving Troullier-Martins (TM) pseudopotentials [35].

The instantaneous density $n(\vec{r},t)$ is given by the sum of all individual electronic orbitals, i.e.,

$$n(\vec{r},t)=\sum_{i=1}^{occ}|\varphi_i(\vec{r},t)|^2. \tag{4}$$

In order to demonstrate the bound states electrons of the projectile, we calculate the projected density of states (PDOS) on the $1s$ orbital of the helium projectile. To show the derivation completely, we also give the definition of the density of

states (DOS)

$$\rho(\varepsilon) = \sum_{i}^{occ} \langle \varphi_i | \varphi_i \rangle \delta(\varepsilon - \varepsilon_i), \tag{5}$$

where ε_i is the eigenvalue of the eigenstate φ_i. Inserting a complete orthonormal basis,

$$1 = \sum_{j} |j\rangle\langle j|, \tag{6}$$

Eq. (5) can be rewritten as

$$\rho(\varepsilon) = \sum_{j} \rho_j(\varepsilon), \tag{7}$$

where $\rho_j(\varepsilon)$ is the PDOS on the j orbital, with

$$\rho_j(\varepsilon) = \sum_{i} \langle \varphi_i | j \rangle \langle j | \varphi_i \rangle \delta(\varepsilon - \varepsilon_i). \tag{8}$$

Energy integrating of the $\rho_j(\varepsilon)$ below Fermi energy multiplied by the occupation number per state gives the number of bound electrons on the j orbital on the particular ion.

The simulations were carried out by using the OCTOPUS *ab initio* real-space code [36,37] and employing the adiabatic local-density approximation with Perdew-Wang analytic parametrization [38] for the time-dependent exchange-correlation potential. There is no basis set in the present work, the external potential, electronic density, and KS orbitals are discretized in a set of mesh grid points with a uniform spacing of 0.18 Å along the three spatial coordinates in the simulation box. A small time step of 0.001 fs is adopted to ensure the stability of the time-dependent computations. Simulations with smaller time steps and grid spacings give essentially the same results.

The host crystalline thin film is an isolated atom cluster, and no periodic boundary condition is employed in this work. To investigate the influence of the initial charge on the final equilibrium charge state under present channeling condition, we performed two kinds of simulations with initial bare and neutral projectile, respectively. In the first case, at the initial stage of simulations, a ground-state DFT calculation is preformed to obtain the converged static state of the host atom cluster. Then the initial bare intruding helium ion is channeled from a point 5 Å above the thin film with given descending velocities along the negative z direction. In the second case, the ground state is achieved with host atom cluster and a helium atom posited at 6 Å above, in the time-dependent run, the helium atom was given an initial velocity downward. For both cases, ionic motion of target atoms is neglected by fixing the host ions in the equilibrium positions as they are expected to play only a marginal role under the well-channeling conditions [39]. The key quantity of interest S_e is extracted by linear fitting the change of the total system energy over the distance after the projectile ions reach equilibrium states in the thin film.

Figure 1 presents position-resolved instantaneous axial force sensed by an initial bare helium ion with velocity of 0.35 a.u. and its instantaneous captured electron number as it is moving through the calculation crystalline thin film. The instantaneous captured electron number is achieved by integrating the PDOS on He-1s orbital over energy range

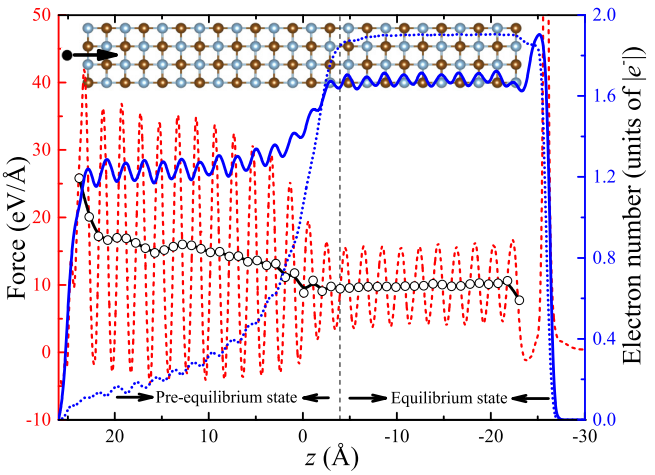

FIG. 1. The evolution the instantaneous axial force (red dashed line) sensed by an initial bare helium ion with velocity of 0.35 a.u. and its instantaneous captured and induced electron numbers (blue dotted and solid lines, respectively) when it is traversing the AlN thin film with thickness of 45.4 Å. The projectile ion moves from $z = 22.7$ to -22.7 Å inside the AlN ⟨100⟩ channel along the main axis. After the ion passing several lattice planes, it reaches charge equilibrium state. The vertical black dashed line shows the position where the projectile reaches equilibrium state. The black circles show the average values of adjacent peaks and valleys of the instantaneous force, and the black line across them shows the trend. The captured electron number is achieved by integrating the He-1s DOS over energy range below Fermi energy. The induced electron number is obtained by integrating the difference between the perturbed and nonperturbed electron density in spheres with radius of 1.26 Å around the flying projectile. The inset shows the sketch of the crystal and projectile at the very beginning of the collision, the gray and green balls denote nitrogen nuclei and allium nuclei, respectively.

below Fermi energy according to Eq. (8). For comparison and to reflect the strength of electronic screening more comprehensively, we also present the instantaneous induced electron number by the projectile helium ion. In the present work, the induced electron is deemed as the mixture of some bound states electrons captured by the initial bare projectile ion and continuum states electrons of the target polarized by the partially neutralized ion, it is obtained by integrating the difference between the time-dependent and the ground-state electron density in a sphere with radius of 1.26 Å around the moving projectile. Such integral radius is carefully chosen, and it is a tradeoff between computational accuracy and phenomenal sensitivity.

As can be seen in Fig. 1, as the slow bare ion gets close to host material, it gradually accumulates electrons, an equilibrium state is achieved after about 11 atom layers. It is to be noted that there are similar trends with the captured electron and the induced electron, indicating the two methods of characterizing the charge state of ions are mutually supportive when reflecting the general changes in trend; the major difference resides in the amplitudes of curves due to different algorithms. Another finding is the instantaneous force on the projectile is quite sensitive to the charge state of the projectile,

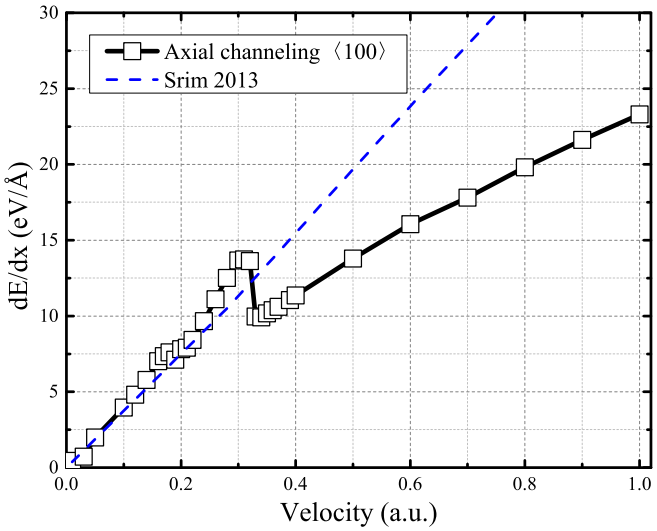

FIG. 2. Electronic stopping power (black open squares) for axially channeled helium ions as a function of velocity along ⟨100⟩ direction, together with the SRIM-2013 predictions (red dashed line). S_e shows local peaks at about 0.17 and 0.31 a.u.. The black solid line is drawn to guide the eyes.

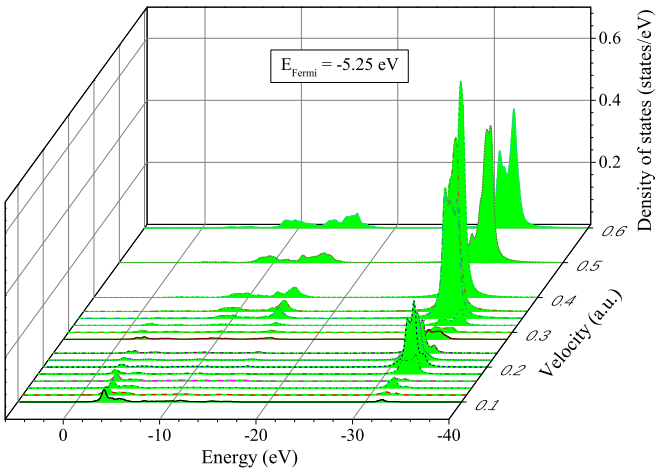

FIG. 3. The instantaneous PDOS on the projectiles with velocities of 0.1 ∼ 0.60 a.u. at $z = -16.7$ Å, respectively, the Fermi energy posits at −5.25 eV.

as the charge accumulation proceeds, the amplitude of instantaneous force sensed by the projectile decreases due to the increase of charge screening from outer electrons. It should be noted that the electron numbers go to zero at $z = -27$ Å, which, corresponding to the location of simulation edge, is due to the OCTOPUS code not allowing any electron escaping the simulation box.

III. RESULTS AND DISCUSSION

A. Implantation of initial bare helium ion

We present in Fig. 2 the simulated S_e results for the motion of helium ions with velocity of 0.01–1.0 a.u. along the midaxis of ⟨100⟩ channel in AlN thin film. Also shown are the predictions from the SRIM-2013 database. The calculated data are extracted by linear fitting the change of the total system energy over the last 6 Å range in conducting solids to keep from the presence of preequilibrium contributions to the stopping. To allow time for the intruding ion getting fully equilibrated during passage through the crystal, which may take several femtoseconds [40], a relatively thick $12 \times 12 \times 52$ Å^3 calculation box, containing a rocksalt AlN $2 \times 2 \times 12$ conventional cell with group number Fm-$3m$ comprising 192 Al and 192 N atoms is employed. The lattice parameter exploited in this work is 3.94 Å, identical to the calculated value by Christensen [41].

As can be seen in Fig. 2, only qualitative agreement between the calculated results and the SRIM predictions is achieved, which can be justified by the fact that SRIM does not explicitly account for any special information of the channeling conditions studied in the present calculations, be it either the ordered lattice structure of the target material, or the local electronic structure [4,16]. The most striking feature of Fig. 2 is that S_e shows two distinctly different trends. Velocity proportionality is valid for relatively high velocity regime ($v > 0.32$ a.u.). While for the velocity range below, local peaks appear at around $v = 0.17$ and 0.31 a.u., such character is obviously inconsistent with the velocity-proportionality assumption.

We have found through direct simulation that S_e responds readily to the charge state of the projectile, which has been reported to have a tremendous effect on the electronic energy loss [42–44]. In a simple intuitive picture: the screening charge around the ion keeps it from rubbing the host electrons directly, which leads to a reduction of the Coulomb interaction between the projectile and the host electrons. Figure 3 present the PDOS on projectile with different velocities at $z = -16.7$ Å. As can be seen, the amplitudes of PDOS major peak at $E = -32$ eV for velocity regime around local stopping peaks are obviously lower than that on both sides, indicating less electrons can be captured by projectile with these velocities.

To show the change of projectile charge states along the trajectory in host material, we present the position-resolved captured electron number by projectile ions in Fig. 4. The ions move from $z = 22.7$ to -22.7 Å inside the AlN crystalline channel. For projectile with velocity of 0.21 a.u., it reaches equilibrium state after traveling about 12 lattice atom planes at $z = -1.0$ Å. For projectile with velocity of 0.4 a.u., it reaches equilibrium state after penetrating about seven lattice atom planes at $z = 9.0$ Å. While for projectile with velocity of 0.16 and 0.32 a.u., which are the velocities closely around stopping peaks, it seems the charge accumulations process are suppressed and no new equilibrium state is found. Basically, for velocity regime away from stopping peaks, new equilibrium states with increased electron number can be achieved after a passage of several lattice atom planes, while it is difficult to achieve charge equilibrium state with enhanced negative charge at or closely around the velocities corresponding to local stopping peaks. It seems that the charge accumulation process is suppressed for projectiles with velocities at or around the stopping peaks.

We also integrate the balance values between the ground-state and time-dependent electron density around the projec-

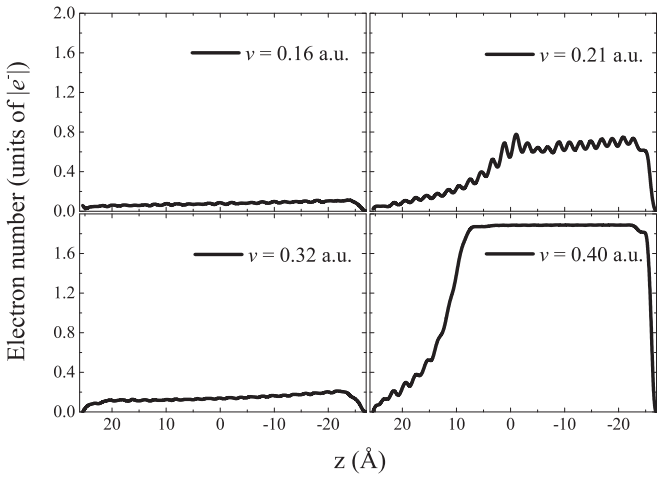

FIG. 4. The position-resolved captured bound electron on axially channelled helium ions with velocities of 0.16, 0.21, 0.32, and 0.40 a.u. along the trajectory in AlN thin film, respectively. The channeling ions move from $z = 22.7$ to -22.7 Å inside AlN along the ⟨100⟩ direction. For velocities away from stopping peaks, i.e., $v = 0.21$ and 0.40 a.u., there are marked electron accumulations on the moving ions at initially stage, then it reaches steady states after the ions traveling certain distance. For velocities closely around stopping peaks, i.e., $v = 0.16$ and 0.32 a.u., only a slight increase of captured electron can be found.

tile to obtain the induced electron number. Figure 5 presents the evolution of the induced electron by projectiles with different velocities along the trajectory of ⟨100⟩ main axis. Consistent with the character of captured electron in Fig. 4, for projectiles with velocities away from stopping peaks, new equilibrium states with increased electron number are achieved after a passage of several lattice atom planes. While the amplitudes of the induced electron for $v = 0.16$ and 0.32 a.u. only change very slightly all through the collision process, and are lower than that of the other velocities.

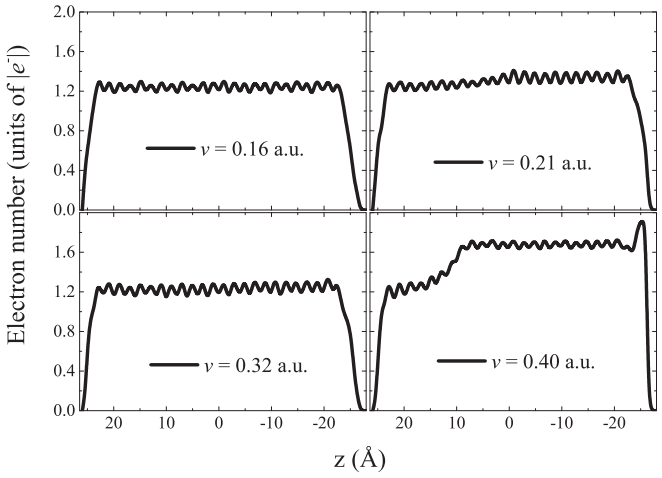

FIG. 5. The position-resolved induced electron on axially channeled helium ions with velocities of 0.16, 0.21, 0.32, and 0.40 a.u. along the trajectory in AlN thin film, respectively. The channeling ions move from $z = 22.7$ to -22.7 Å inside AlN along the ⟨100⟩ direction.

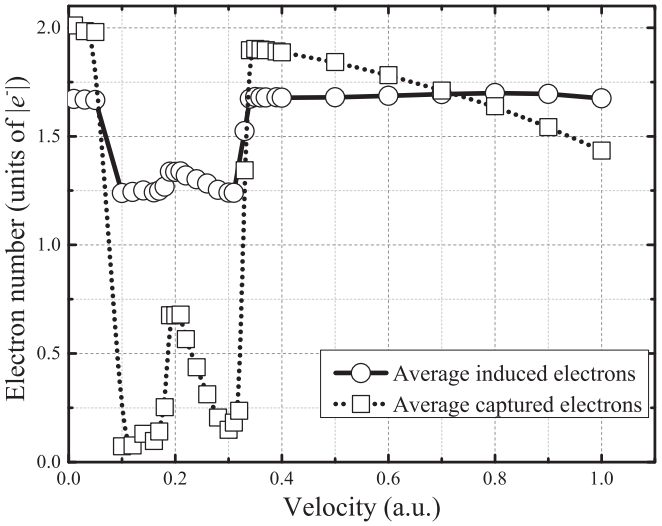

FIG. 6. Velocity-resolved average induced electron and captured electron on axially channeled helium ions at steady states. See more details in the text. The line are drawn to guide the eyes.

To reflect the velocity-resolved electronic screening by the charges on the projectile, we present in Fig. 6 the average induced and captured electron, respectively, by the projectiles over the last 6 Å ionic range in crystal, i.e., from $z = -16.7$ to $z = -22.7$ Å. Contrary to the trend of S_e versus velocity shown in Fig. 2, there are valleys for the induced and captured electron at around $v = 0.17$ and 0.31 a.u., and two steep slopes follow closely the valleys. The charges reach relative steady states at velocity regime above 0.33 a.u., and no nonlinear S_e occurs in this regime. The synchronous and inverse trend of charge and S_e suggests the nonlinear phenomenon at relatively low velocity regime in Fig. 2 is caused by the odd effective charge behavior.

There is another finding in Fig. 6, the amplitude of captured electron is much lower than that of the induced electron in the valley, suggesting considerable number of target continuum states charges are polarized around the highly stripped ions. It is to be noted that, although the captured bound states electrons relative with the charge state of the projectile more directly, the screening effects by the polarized target continuum states electrons also contribute to the electronic stopping [45], since the Hellman-Feynman force, which is the key variable in describing the nonadiabatic coupling of electron ion, do not distinguish between an electron belonging to the projectile or target atoms. Thus, from the perspective of charge screening, the induced electron is more meaningful than the captured electron in some sense. In present work, we found a periodic charge oscillation phenomenon as the intruding ion channeling through the AlN thin film, where the induced electron around the projectile oscillates back and forth due to field generated by the crystal layer, the oscillation frequency depends on the ions passage between equivalent ionic configurations. The oscillation frequency is defined as $\omega = 2\pi|v|/d$, where d is distance between tetrahedral points in the ⟨100⟩ channel, v is the projectile velocity. We present in Fig. 7 the snapshots of charge oscillation process for helium ion penetrating a host cluster with 384 atoms. At $t = 4.39$ fs,

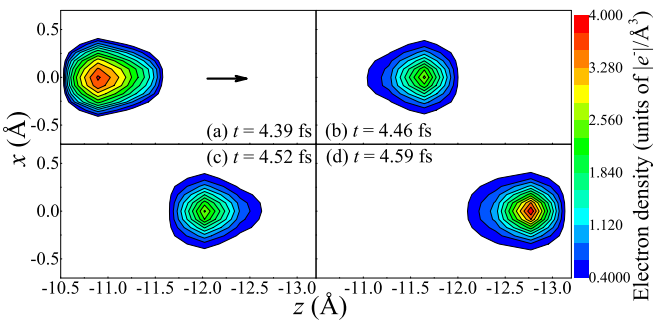

FIG. 7. Oscillation of induced electron around the channeling ion with velocity of 0.31 a.u., the ion is traveling left to right along the main axis of ⟨100⟩ channel. (a)–(d) are four consecutive snapshots with interval of about 0.07 fs.

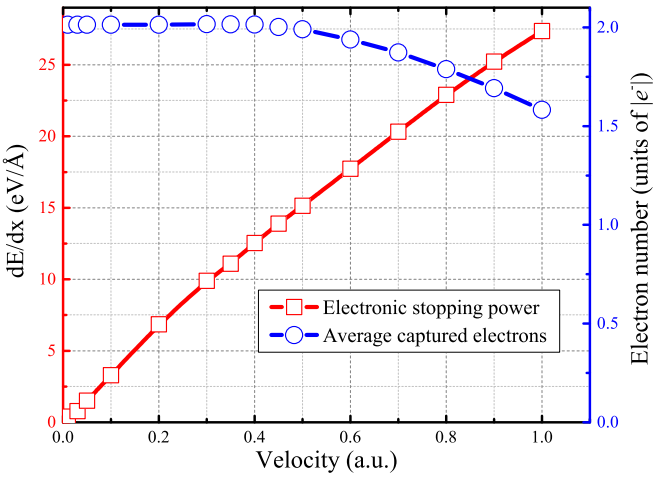

FIG. 8. Velocity-resolved average captured bound electron and electronic stopping for initial bare projectile along random trajectory. The red squares represent electronic stopping power for helium moves along the ⟨100⟩ direction in AlN thin film. The blue hollow circles represent velocity-resolved average captured electron on axially channeled helium ions at steady states. The lines are drawn to guide the eyes.

the instantaneous distribution of induced electron is skewed to the left, 0.07 fs later at $t = 4.46$ fs, the charge distribution shifts to the right; similar transition repeats in the following process at $t = 4.52$ and 4.59 fs. It is to be noted that such charge oscillation due to the space-periodic field from lattice atoms is absent in the linear response models [46–48], where the induced electron lags behind the projectile and forms the wake potential.

The counterintuitive behavior of charge state in the low velocity regime is attributed to the charge resonance, that is when the charge oscillation resonates with the charge state on the projectile, it would depress the formation of defect state on the projectile, which furthermore keeps the initial bare intruding ion capturing electrons. Similar resonance phenomenon has also been reported by Mason and Race for self-irradiated Cu [8]. Using time-dependent tight-binding model, they observed a resonant charging phenomenon in the valence electron states for self-irradiated Cu, and they found an enhancement of negative charge on the channeling ion at narrow velocity window. Such result was interpreted as a consequence of the resonant excitation of electrons in delocalized states near the Fermi energy onto the defect states above Fermi energy localized on the channeling ion during passage through the host matter.

To verify the correlation between the strange electronic behavior and the atomic arrangement dependent charge resonance, we calculated the electronic stopping and charge state of channeling ion along random trajectory, where no periodic charge oscillation occurs. The results are presented in Fig. 8. As can be seen, neither local valleys for induced and captured electron nor local peaks for electronic stopping occurs all through the velocity regime we considered.

B. Neutral projectile channeling

In such case, we use an initial condition that represents neutral (or fully screened) projectiles from the solution of the ground-state KS equations with the projectile included in the external potential. The projectile atom is initially placed at 6 Å from the top layer of the host atoms to prevent the interference of the projectile and the host atoms. Thus for system with the same target atom cluster size, a relatively larger simulation box than for initial bare ion case has to be employed. Considering that PDOS calculation is very computation consuming, we performed such calculations in a $2 \times 2 \times 10$ conventional cell with 320 host atoms, smaller than the one used in Sec. III A with 384 host atoms. When the time-dependent process begins, the projectile atom is given an initial velocity downward. We present in Fig. 9 the velocity-resolved PDOS on projectile at $z = -16.7$ Å, different from the case for initial bare projectile shown in Fig. 3, the amplitudes of PDOS are not suppressed for velocity regime around certain velocity. We also show in Figs. 10 and 11 the change of the captured and induced electron on projectile with different velocities along the trajectory of ⟨100⟩ main axis. As can be seen, for projectiles with all the velocities, they reach equilibrium states soon after entering the host thin film. Unlike the trend in Figs. 4 and 5, both the induced electron and captured electron

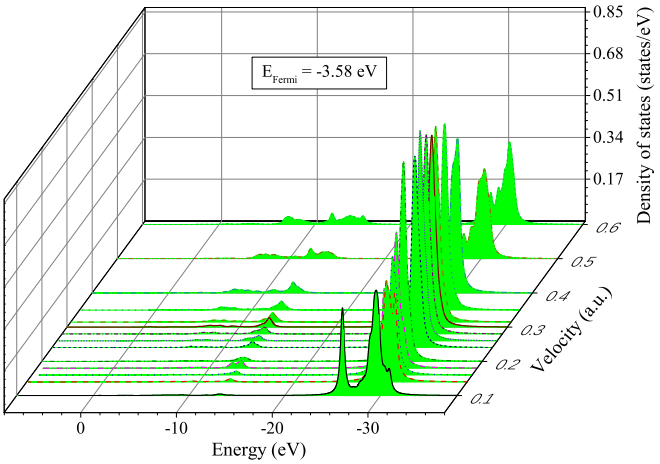

FIG. 9. The instantaneous PDOS on the projectiles with velocities of 0.1 ∼ 0.60 a.u. at $z = -16.7$ Å, respectively, the Fermi energy posits at −3.58 eV.

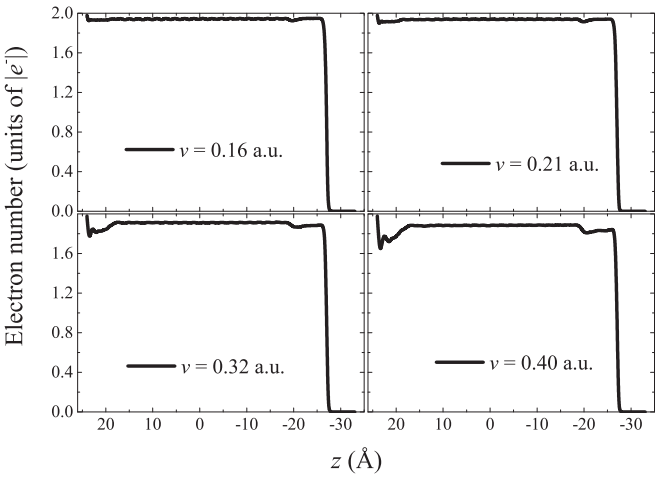

FIG. 10. The position-resolved bound electron on axially channeled helium ions with velocities of 0.16, 0.21, 0.32, and 0.40 a.u. along the trajectory in AlN thin film, respectively. The channeling ions move from $z = 18.8$ to -18.8 Å inside AlN along the ⟨100⟩ direction.

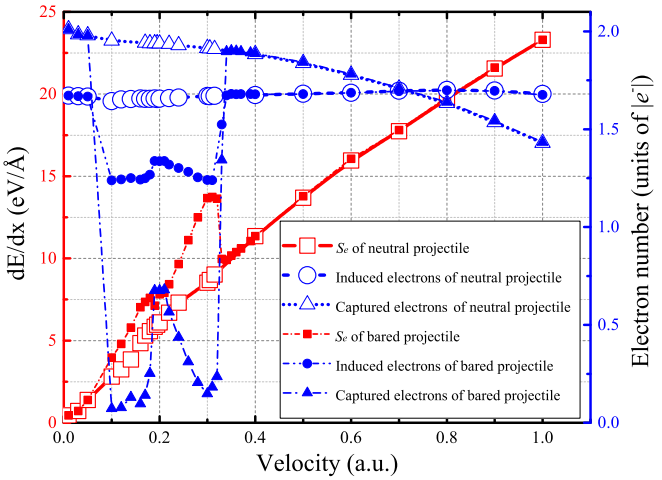

FIG. 12. Velocity-resolved charge states and electronic stopping for initial neutral and bare projectile, respectively. The red squares represent electronic stopping power for helium moves along the ⟨100⟩ direction in AlN thin film. The blue hollow triangles and circles represent velocity-resolved average induced and captured electron, respectively, on axially channeled helium ions at steady states. See more details in the text. The lines are drawn to guide the eyes.

are not depressed at characteristic velocities of 0.17 and 0.31, the charge states just keep constant in the following process, suggesting the charge resonance make marginal effect on the charge state of initial neutral incident ion.

Figure 12 demonstrates the electronic stopping and the velocity-resolved average captured and induced electron for initially neutral ion with hollow symbols, for comparison, the corresponding results for initial bare ion, which have been shown in Figs. 2 and 6, are also presented with solid symbols in Fig. 12. As can be seen, neither local valleys for induced and captured electron nor local peaks for electronic stopping occurs near characteristic velocities of 0.17 and 0.31 a.u.. It can be concluded that REC in the present work only take effect on the charge accumulation of highly charged incident ion near characteristic velocities, while not make significant influence on the excitation of bound states charge.

We noticed that, for initial bare ion, although in velocity regime around characteristic velocities of 0.17 and 0.31 a.u., the amplitudes of final charge are suppressed to varied degrees, while there is almost no discrepancy in the electronic stopping and final charge states with neutral incident ions at $v > 0.32$ a.u.. Thus, if it is not affected by the charge resonance, the charge states of the projectiles only depend on the instantaneous velocities after a passage of several atom lattices when they reach equilibrium states, and are independent

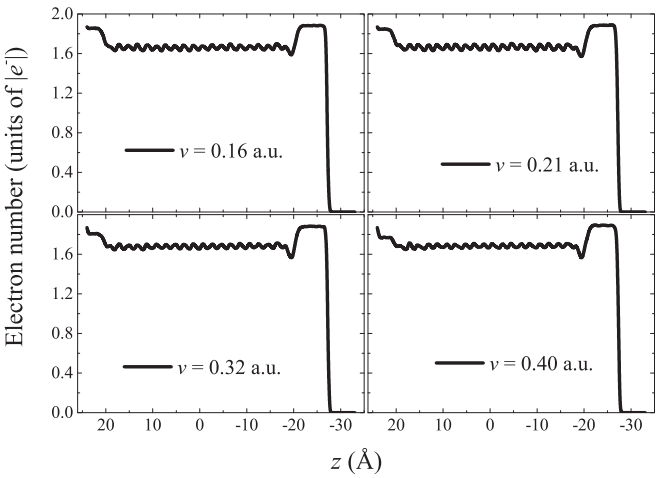

FIG. 11. The position-resolved induced electron on axially channeled helium ions with velocities of 0.16, 0.21, 0.32, and 0.40 a.u. along the trajectory in AlN thin film, respectively. The channeling ions move from $z = 18.8$ to -18.8 Å inside AlN along the ⟨100⟩ direction.

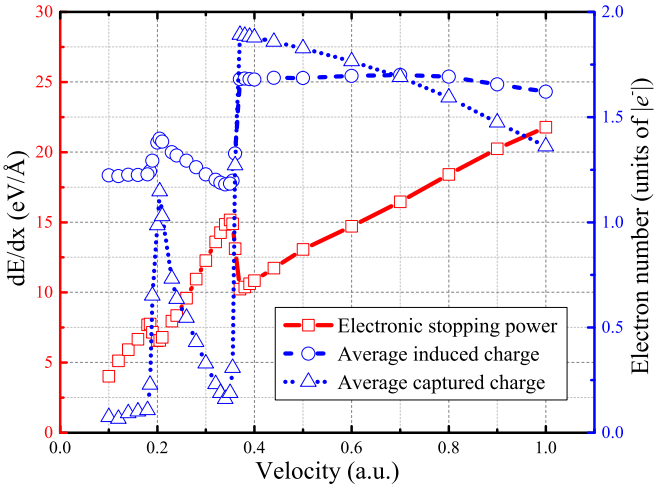

FIG. 13. The red squares represent electronic stopping power for helium ions move along the ⟨100⟩ direction in AlN thin film with lattice parameters increased by 10% in the incident direction. The blue hollow triangles and circles represent velocity-resolved average induced and captured electron respectively on axially channelled helium ions at steady states. The lines are drawn to guide the eyes.

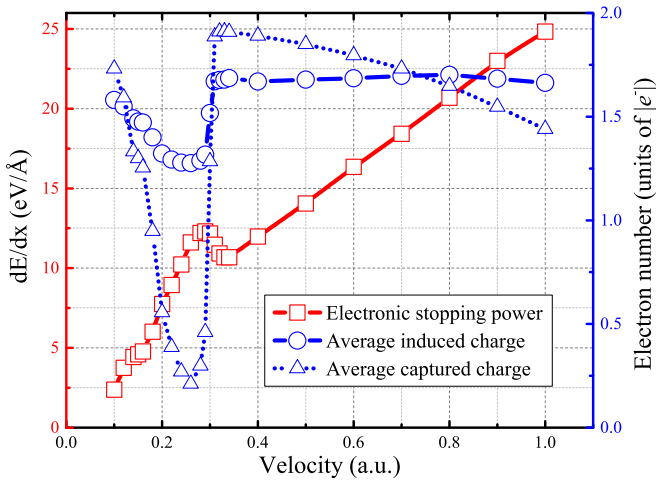

FIG. 14. The red squares represent electronic stopping power for helium ion moves along the ⟨100⟩ direction in AlN thin film with lattice parameters decreased by 10% in the incident direction. The blue hollow triangles and circles represent velocity-resolved average induced and captured electron respectively on axially channeled helium ions at steady states. The lines are drawn to guide the eyes.

of incident charge states. A similar conclusion was reached by Lee *et al.* [19].

C. Channeling with revised lattice parameters

In order to make a further exploration to the structural relevance of charge resonance, we also investigated the S_e and effective charge of helium ion moving in AlN crystalline lattice with lattice parameters increased and decreased by 10% in the incident direction along main axis of ⟨100⟩ channel, respectively, for which the distances between lattice planes along the ion trajectory are about 10% higher or lower than that of real crystal.

Figures 13 and 14 present the S_e and charge of helium ion implanted along the main axis of ⟨100⟩ channel AlN crystalline lattice with lattice parameter increased and decreased by 10% in the incident direction, respectively. It demonstrates in Figs. 13 and 14 that, though the amplitudes of S_e is different from that in real crystal, similar nonlinear S_e trends in low velocity regime also appear; there are major local peaks at about $v = 0.28$ and 0.35 a.u., respectively. Local valleys of charge also occur at around $v = 0.28$ and 0.35 a.u., which additionally reflects the S_e has a direct relation with effective charge, and indicates 0.28 and 0.35 a.u. are characteristic velocities of charge resonance where the ionic charge is effectively excited under the present channeling condition. It is noteworthy that the velocities corresponding to S_e peaks in channel with revised lattice parameter are about 10% different from the characteristic velocities in real crystal channeling cases, in line with the difference of the spacing between the real and revised crystalline lattice, which furthermore suggests the existence of the aforementioned quantitative space-periodic potential.

IV. CONCLUSIONS

We report theoretical study from first principles the nonadiabatic interaction of slow helium ions with rocksalt crystalline AlN cluster. It is found electronic energy loss is quite sensitive to charge states of the projectile. Our TDDFT calculations show that under channeling conditions the periodic lattice atoms have a nontrivial influence on the effective charge of the low-velocity projectile by depressing the formation of defect states on the projectile, which furthermore results in the change of the slope for electronic stopping versus velocity. We have also shown the charge revolution of the initially neutral projectile, by comparing with that of initial bare incident ion, and we reach the conclusion that the effect of charge resonance mainly resides in the charge accumulation process of highly charged projectile while having marginal influence on the excitation of occupied state charge. Furthermore, we found the final charge states of the projectiles are independent of the initial charge state of incident ion in velocity regime away from characteristic velocities of charge resonance.

The quantitative coincidence of the change of local peaks of S_e and lattice parameters indicates the nonlinear stopping in this work is in correlation with the lattice atom distribution, which is beyond the frame of free electron gas and linear response approximations that treat the electronic structure of lattice atom implicitly.

ACKNOWLEDGMENTS

This work was supported by National Natural Science Foundation of China under Grants No. 12135002 and No. 12105205, China Postdoctoral Science Foundation (Grants No. 2019M662693, No. 2020T130486, and No. 2021M700003).

[1] B. Domeij, F. Brown, J. A. Davies, G. R. Piercy, and E. V. Kornelsen, Phys. Rev. Lett. **12**, 363 (1964).
[2] T. Furuya, H. Nishi, T. Inada, and T. Sakurai, J. Appl. Phys. **49**, 3918 (1978).
[3] T. D. D. L. Rubia, Mater. Res. **26**, 613 (1996).
[4] E. E. Quashie, B. C. Saha, and A. A. Correa, Phys. Rev. B **94**, 155403 (2016).
[5] D. Cai, N. Gronbech-Jensen, C. M. Snell, and K. M. Beardmore, Phys. Rev. B **54**, 17147 (1996).
[6] G. Hobler, A. Simionescu, L. Palmetshofer, C. Tian, and G. Stingeder, J. Appl. Phys. **77**, 3697 (1995).
[7] R. Bernabei, P. Belli, F. Montecchia, F. Nozzoli, F. Cappella, A. Incicchitti, D. Prosperi, R. Cerulli, C. Dai, H. He *et al.*, Eur. Phys. J. C **53**, 205 (2008).
[8] D. R. Mason, C. P. Race, M. H. F. Foo, A. P. Horsfield, W. M. C. Foulkes, and A. P. Sutton, New J. Phys. **14**, 073009 (2012).
[9] M. Draxler, S. P. Chenakin, S. N. Markin, and P. Bauer, Phys. Rev. Lett. **95**, 113201 (2005).
[10] D. Roth, B. Bruckner, G. Undeutsch, V. Paneta, A. I. Mardare, C. L. McGahan, M. Dosmailov, J. I. Juaristi, M. Alducin, J. D. Pedarnig, R. F. Haglund, D. Primetzhofer, and P. Bauer, Phys. Rev. Lett. **119**, 163401 (2017).

[11] S. N. Markin, D. Primetzhofer, and P. Bauer, Phys. Rev. Lett. **103**, 113201 (2009).
[12] K. Eder, D. Semrad, P. Bauer, R. Golser, P. Maier-Komor, F. Aumayr, M. Peñalba, A. Arnau, J. M. Ugalde, and P. M. Echenique, Phys. Rev. Lett. **79**, 4112 (1997).
[13] A. Lim, W. M. C. Foulkes, A. P. Horsfield, D. R. Mason, A. Schleife, E. W. Draeger, and A. A. Correa, Phys. Rev. Lett. **116**, 043201 (2016).
[14] J. Lindhard, A. Winther *et al.*, *Stopping Power of Electron Gas and Equipartition Rule* (Munksgaard, Copenhagen, 1964).
[15] A. A. Correa, Comput. Mater. Sci. **150**, 291 (2018).
[16] A. Schleife, Y. Kanai, and A. A. Correa, Phys. Rev. B **91**, 014306 (2015).
[17] H. Bethe, Annalen der Physik **397**, 325 (1930).
[18] J. Lindhard and M. Scharff, Phys. Rev. **124**, 128 (1961).
[19] C.-W. Lee, J. A. Stewart, R. Dingreville, S. M. Foiles, and A. Schleife, Phys. Rev. B **102**, 024107 (2020).
[20] A. Kononov and A. Schleife, Phys. Rev. B **102**, 165401 (2020).
[21] P. Echenique, R. Nieminen, and R. Ritchie, Solid State Commun. **37**, 779 (1981).
[22] P. M. Echenique, R. M. Nieminen, J. C. Ashley, and R. H. Ritchie, Phys. Rev. A **33**, 897 (1986).
[23] R. Ullah, F. Corsetti, D. Sánchez-Portal, and E. Artacho, Phys. Rev. B **91**, 125203 (2015).
[24] F. Mao, C. Zhang, J. Dai, and F.-S. Zhang, Phys. Rev. A **89**, 022707 (2014).
[25] M. Caro, A. Tamm, A. Correa, and A. Caro, J. Nucl. Mater. **507**, 258 (2018).
[26] C.-K. Li, F. Wang, B. Liao, X.-P. OuYang, and F.-S. Zhang, Phys. Rev. B **96**, 094301 (2017).
[27] S. Nakagawa, Phys. Status Solidi B **178**, 87 (1993).
[28] S. Lohmann, R. Holeňák, and D. Primetzhofer, Phys. Rev. A **102**, 062803 (2020).
[29] S. Lohmann and D. Primetzhofer, Phys. Rev. Lett. **124**, 096601 (2020).
[30] S. Datz, C. D. Moak, O. H. Crawford, H. F. Krause, P. F. Dittner, J. Gomez del Campo, J. A. Biggerstaff, P. D. Miller, P. Hvelplund, and H. Knudsen, Phys. Rev. Lett. **40**, 843 (1978).
[31] V. V. Okorokov, Yadern Fiz **2**, 349 (1965).
[32] V. V. Okorokov, ZhETF Pisma Redaktsiiu **2**, 175 (1965).
[33] S. Shindo and Y. H. Ohtsuki, Phys. Rev. B **14**, 3929 (1976).
[34] X. Andrade, A. Castro, D. Zueco, J. L. Alonso, P. Echenique, F. Falceto, and A. Rubio, J. Chem. Theory Comput. **5**, 728 (2009).
[35] N. Troullier and J. L. Martins, Phys. Rev. B **43**, 1993 (1991).
[36] M. A. L. Marques, A. Castro, G. F. Bertsch, and A. Rubio, Comput. Phys. Commun. **151**, 60 (2003).
[37] A. Castro, H. Appel, M. Oliveira, C. A. Rozzi, X. Andrade, F. Lorenzen, M. A. L. Marques, E. K. U. Gross, and A. Rubio, Phys. Status Solidi B **243**, 2465 (2006).
[38] J. P. Perdew and Y. Wang, Phys. Rev. B **45**, 13244 (1992).
[39] A. A. Correa, J. Kohanoff, E. Artacho, D. Sánchez-Portal, and A. Caro, Phys. Rev. Lett. **108**, 213201 (2012).
[40] M. Hattass, T. Schenkel, A. V. Hamza, A. V. Barnes, M. W. Newman, J. W. McDonald, T. R. Niedermayr, G. A. Machicoane, and D. H. Schneider, Phys. Rev. Lett. **82**, 4795 (1999).
[41] N. E. Christensen and I. Gorczyca, Phys. Rev. B **47**, 4307 (1993).
[42] J. I. Juaristi, A. Arnau, P. M. Echenique, C. Auth, and H. Winter, Phys. Rev. Lett. **82**, 1048 (1999).
[43] W. Brandt and M. Kitagawa, Phys. Rev. B **25**, 5631 (1982).
[44] G. D. Sauter and S. D. Bloom, Phys. Rev. B **6**, 699 (1972).
[45] L. W. Campbell, Phys. Rev. B **102**, 245103 (2020).
[46] J. Lindhard, Dan. Vid. Selsk Mat.-Fys. Medd. **28**, 8 (1954).
[47] R. H. Ritchie, Phys. Rev. **114**, 644 (1959).
[48] P. M. Echenique, F. Flores, and R. H. Ritchie, Dynamic screening of ions in condensed matter, *Solid State Physics*, Vol. 43 (Academic Press, New York, 1990), pp. 229–308.